Chapter 3: Traditional Artificial Potential Field

3.1 Introduction to Potential Functions

Potential functions are mathematical tools used to represent a robot's environment as an energy landscape. They direct the robot's motion by defining attractive and repulsive forces that guide it toward a goal while avoiding obstacles. This approach uses a gradient-descent method, where the robot follows the direction of the steepest decrease in potential energy. The potential function is defined as a real-valued function $U : \mathbb{R}^m \to \mathbb{R}$, which assigns an energy value to each point in the configuration space. The theoretical foundation of this approach is detailed by Choset in [2], where the concepts of potential functions for robotic motion planning are discussed extensively.

3.2 Components of the Potential Function

The potential function $U(q)$ is typically composed of two parts: attractive and repulsive potentials.

Attractive Potential

The attractive potential $U_{\text{att}}(q)$ is designed to pull the robot toward the goal q_{goal}. A well-constructed attractive potential ensures that its value increases monotonically with the distance to the goal $d(q, q_{\text{goal}})$, and the negative gradient of this potential directs the robot along the path to the goal.

The simplest form of the attractive potential is the **conic potential**, defined as:

$$U_{\text{att}}(q) = \zeta d(q, q_{\text{goal}}), \tag{3.1}$$

where ζ is a scaling parameter that determines the strength of attraction, and $d(q, q_{\text{goal}}) = \|q - q_{\text{goal}}\|$ is the Euclidean distance between the robot's current position q and the goal q_{goal}. The gradient of the conic potential is:

$$\nabla U_{\text{att}}(q) = \zeta \frac{q - q_{\text{goal}}}{d(q, q_{\text{goal}})}. \tag{3.2}$$

The behavior of the **conic potential** can be visualized in Figure 3.1. As shown, the potential increases linearly with the distance to the goal q_{goal}, forming a conical surface.

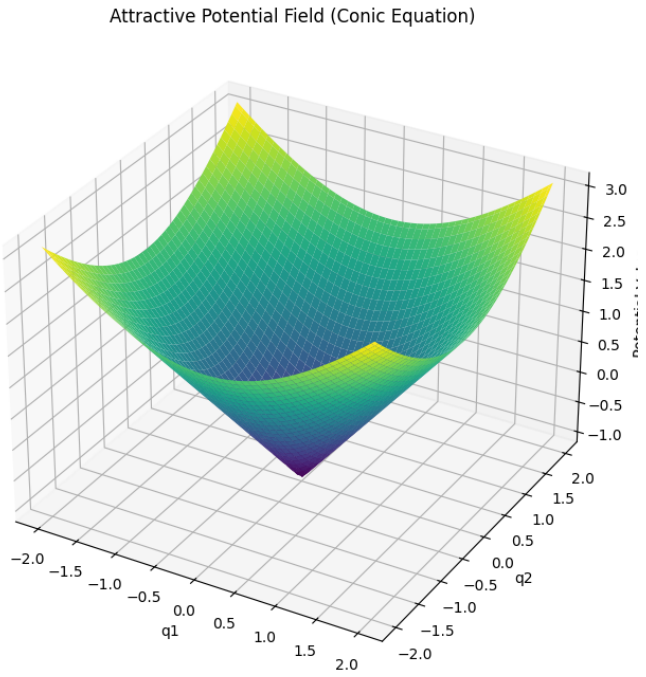

Figure 3.1: Visualization of the Conic Attractive Potential

However, the discontinuity in the gradient of the conic potential near q_{goal} can cause instability. To address this, the **quadratic potential** is introduced (Figure 3.2). It grows quadratically with the distance, ensuring a smooth gradient and more stable robot motion near the goal.

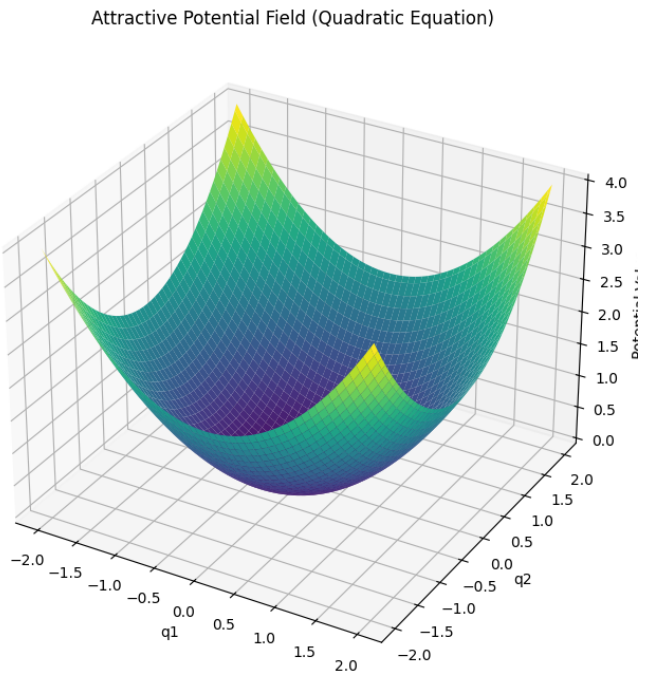

Figure 3.2: Visualization of the Quadratic Attractive Potential

With equation:

$$U_{\text{att}}(q) = \frac{1}{2}\zeta d^2(q, q_{\text{goal}}). \tag{3.3}$$

The gradient of the quadratic potential is:

$$\nabla U_{\text{att}}(q) = \zeta(q - q_{\text{goal}}). \tag{3.4}$$

To balance the strengths of the conic and quadratic potentials, a hybrid approach (Figure 3.3) combines the two, switching between them at a threshold distance d^*_{goal}:

$$U_{\text{att}}(q) = \begin{cases} \frac{1}{2}\zeta d^2(q, q_{\text{goal}}), & d(q, q_{\text{goal}}) \leq d^*_{\text{goal}}, \\ \zeta d^*_{\text{goal}} d(q, q_{\text{goal}}) - \frac{1}{2}\zeta (d^*_{\text{goal}})^2, & d(q, q_{\text{goal}}) > d^*_{\text{goal}}. \end{cases} \tag{3.5}$$

The gradient for the hybrid potential is:

$$\nabla U_{\text{att}}(q) = \begin{cases} \zeta(q - q_{\text{goal}}), & d(q, q_{\text{goal}}) \leq d^*_{\text{goal}}, \\ \frac{\zeta d^*_{\text{goal}}}{d(q, q_{\text{goal}})}(q - q_{\text{goal}}), & d(q, q_{\text{goal}}) > d^*_{\text{goal}}. \end{cases} \tag{3.6}$$

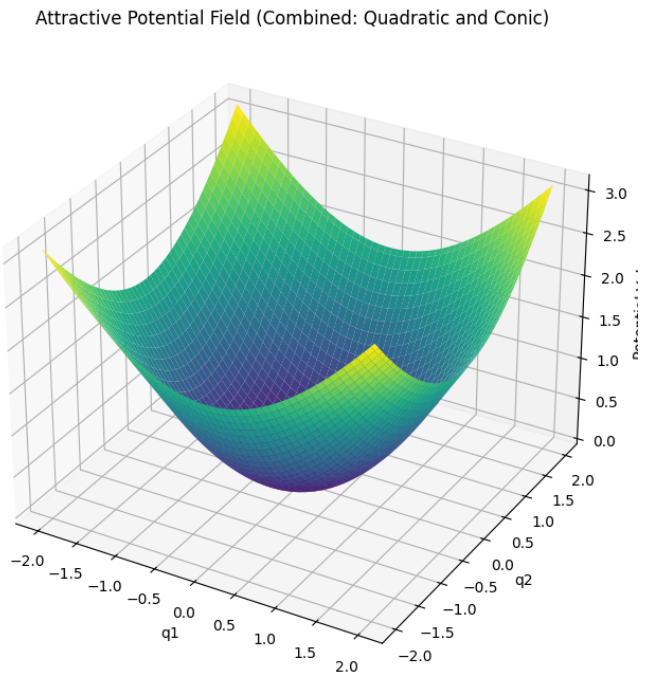

Figure 3.3: Visualization of the Combined Attractive Potential

Repulsive Potential

The repulsive potential $U_{\text{rep}}(q)$ generates forces to steer the robot away from obstacles. When there are multiple obstacles, the repulsive potential is the sum of potentials from each individual obstacle:

$$U_{\text{rep}}(q) = \sum_{i=1}^{n} U_{\text{rep},i}(q), \tag{3.7}$$

where $U_{\text{rep},i}(q)$ is the repulsive potential for the i-th obstacle.

$$U_{\text{rep},i}(q) = \begin{cases} \frac{1}{2}\eta \left(\frac{1}{d_i(q)} - \frac{1}{Q_i^*}\right)^2, & \text{if } d_i(q) \leq Q_i^*, \\ 0, & \text{if } d_i(q) > Q_i^*, \end{cases} \tag{3.8}$$

The gradient of the repulsive potential is given by:

$$\nabla U_{\text{rep},i}(q) = \begin{cases} \eta \left(\frac{1}{Q_i^*} - \frac{1}{d_i(q)}\right) \frac{1}{d_i^2(q)} \nabla d_i(q), & \text{if } d_i(q) \leq Q_i^*, \\ 0, & \text{if } d_i(q) > Q_i^*, \end{cases} \tag{3.9}$$

where the $Q_i^* \in \mathbb{R}$ domain of influence of each obstacle, and the η can be viewed as

a gain on the repulsive gradient. Assuming convex obstacles, the distance $d_i(q)$ is the minimum distance from q to the surface of the i-th obstacle:

$$d_i(q) = \min_{c \in O_i} \|q - c\|, \tag{3.10}$$

where O_i represents the set of points on the i-th obstacle's boundary. The corresponding gradient is:

$$\nabla d_i(q) = \frac{q - c}{d(q, c)}, \tag{3.11}$$

where c is the closest point on the obstacle to q. The gradient of the total repulsive potential becomes:

$$\nabla U_{\text{rep}}(q) = \sum_{i=1}^{n} \nabla U_{\text{rep},i}(q). \tag{3.12}$$

Figure 3.4 bellow illustrates the magnitude of the repulsive gradient 3.9 as a function of the distance to an obstacle $d(q, O)$. When the distance to the obstacle is greater than the threshold Q^*, the repulsive gradient becomes zero, meaning the obstacle has no influence on the robot. However, as the distance decreases below the threshold, the magnitude of the gradient increases significantly, pushing the robot away from the obstacle.

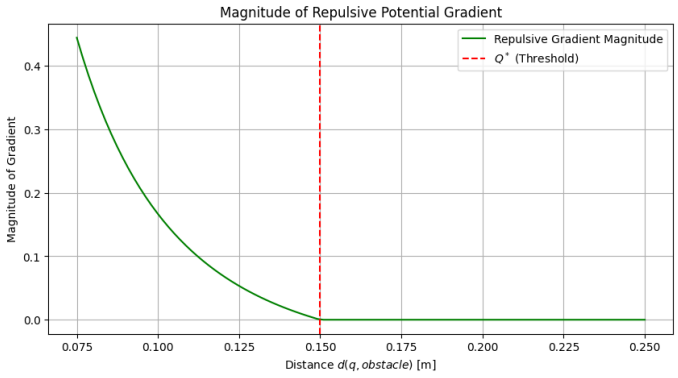

Figure 3.4: Magnitude of the Repulsive Gradient

Combined Potential Function

The total potential function combines the attractive 3.5 and repulsive 3.7 potentials:

$$U(q) = U_{\text{att}}(q) + U_{\text{rep}}(q). \tag{3.13}$$

as seen in the figure below.

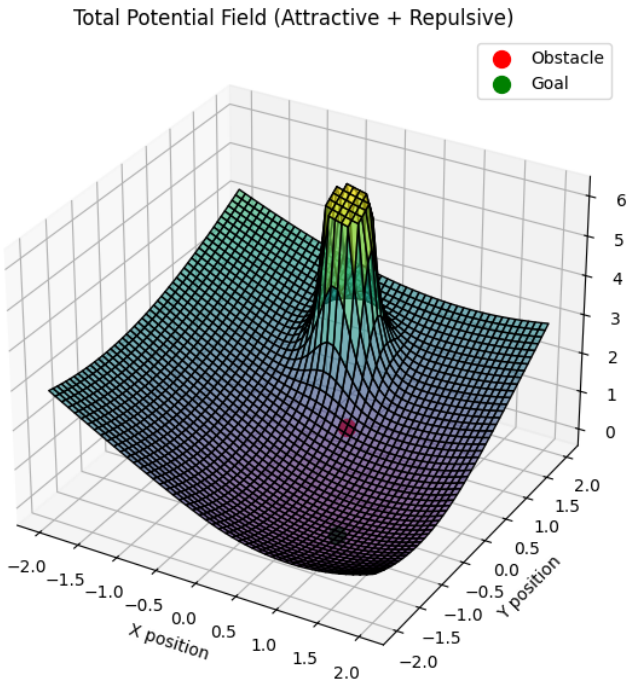

Figure 3.5: Visualization of the Total Potential

The robot follows the negative gradient of $U(q)$ 3.13, moving in the direction of steepest descent to minimize the total potential. The resulting force field is:

$$F(q) = -\nabla U(q) = -\nabla U_{\text{att}}(q) - \nabla U_{\text{rep}}(q). \tag{3.14}$$

There are three main ways to use this force for motion planning:

1. **Force Control**: Treat $F(q)$ as a generalized force that directly drives the robot's motion based on its dynamics.

2. **Acceleration-Based Control**: Consider $F(q)$ as a force applied to a unit mass, resulting in an acceleration of the robot.

3. **Velocity-Based Control**: Use $F(q)$ as a velocity vector that directly dictates the robot's movement.

3.3 Extension to Rigid-Body Robots and Articulated Manipulators

Extension to Rigid-Body Robots

The application of potential functions to rigid-body robots extends the general framework by incorporating the robot's geometry. Instead of treating the robot as a single point, we use **control points**, key positions on the robot's structure, to approximate its interaction with the environment, as shown in figure 3.6 bellow.

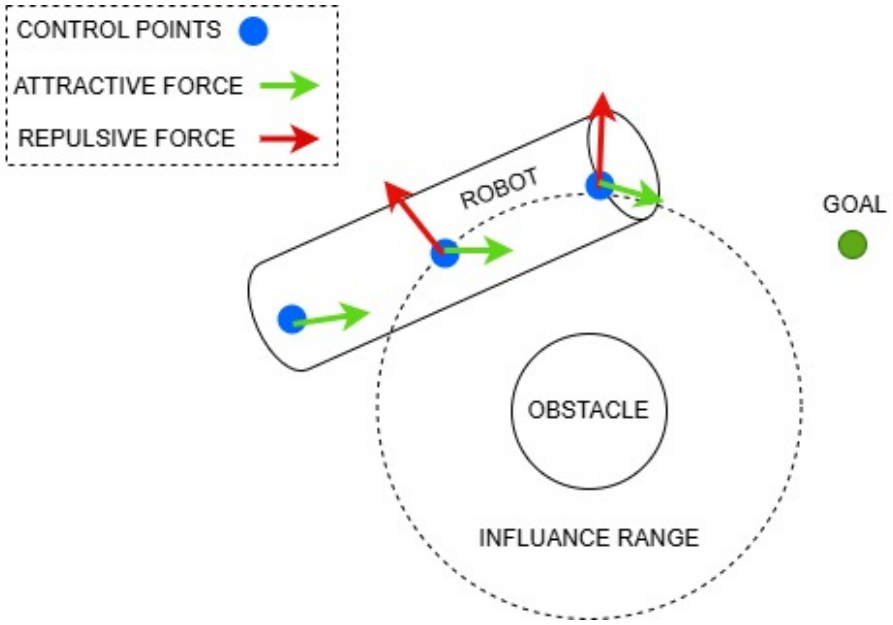

Figure 3.6: Rigid-Body Robot Control Points

Attractive Potential for Rigid Bodies

For each control point r_j, the attractive potential guides it toward its target position $r_j(q_{\text{goal}})$.

$$U_{\text{att},j}(q) = \begin{cases} \frac{1}{2}\zeta_j d^2(r_j(q), r_j(q_{\text{goal}})), & d(r_j(q), r_j(q_{\text{goal}})) \leq d^*_{\text{goal}}, \\ \zeta_j d^*_{\text{goal}} d(r_j(q), r_j(q_{\text{goal}})) - \frac{1}{2}\zeta_j (d^*_{\text{goal}})^2, & \text{otherwise.} \end{cases} \tag{3.15}$$

The gradient of this potential, which provides the attractive force for the control

point, is:

$$\nabla U_{\text{att},j}(q) = \begin{cases} \zeta_j(r_j(q) - r_j(q_{\text{goal}})), & d(r_j(q), r_j(q_{\text{goal}})) \leq d^*_{\text{goal}}, \\ \frac{\zeta_j d^*_{\text{goal}}}{d(r_j(q), r_j(q_{\text{goal}}))}(r_j(q) - r_j(q_{\text{goal}})), & \text{otherwise.} \end{cases} \tag{3.16}$$

Repulsive Potential for Rigid Bodies

The repulsive potential now accounts for the shortest distance between each control point r_j and nearby obstacles W_{O_i}:

$$U_{\text{rep},j,i}(q) = \begin{cases} \frac{1}{2}\eta_j \left(\frac{1}{d_i(r_j(q))} - \frac{1}{Q^*_i}\right)^2, & d_i(r_j(q)) \leq Q^*_i, \\ 0, & \text{otherwise.} \end{cases} \tag{3.17}$$

The gradient of this potential, representing the repulsive force for the control point, is:

$$\nabla U_{\text{rep},j,i}(q) = \begin{cases} \eta_j \left(\frac{1}{Q^*_i} - \frac{1}{d_i(r_j(q))}\right) \frac{1}{d_i^2(r_j(q))} \nabla d_i(r_j(q)), & d_i(r_j(q)) \leq Q^*_i, \\ 0, & \text{otherwise.} \end{cases} \tag{3.18}$$

Here, $d_i(r_j(q))$ is the shortest distance between the control point r_j and the obstacle W_{O_i}, and $\nabla d_i(r_j(q))$ is a unit vector pointing away from the obstacle (similarly to equations 3.10 and 3.11).

Path Planning for Articulated Manipulators

Path planning for articulated manipulators is a crucial challenge due to the high-dimensional configuration spaces and rotational degrees of freedom (DOFs). Both Choset [3] and Siciliano [4] propose a similar method: control points distributed on the manipulator, generate attractive forces toward the goal and repulsive forces away from obstacles. These workspace forces are mapped to configuration space using Jacobians, allowing the convert into joint torques or velocities.

Challenges of Potential Functions

While computationally efficient and intuitive, potential functions face several challenges:

- **Local Minima:** The robot can get trapped in undesired local minima where $\nabla U(q) = 0$, preventing it from reaching the goal.
- **Oscillations:** Discontinuities in the gradient may cause the robot to oscillate, particularly in narrow passages.
- **Incomplete Planning:** In environments with complex obstacles, the method may fail to find a path to the goal.

3.4 Implementation of T-APF in the Kinova Arm

In our implementation of the Traditional Artificial Potential Field (T-APF) method, we adopt a velocity-based control approach. The artificial potential field is established in Cartesian space at multiple control points distributed along the robot arm, as illustrated in Figure 3.7 and detailed in Table 3.1. The potential field forces at each control point are interpreted as velocities.

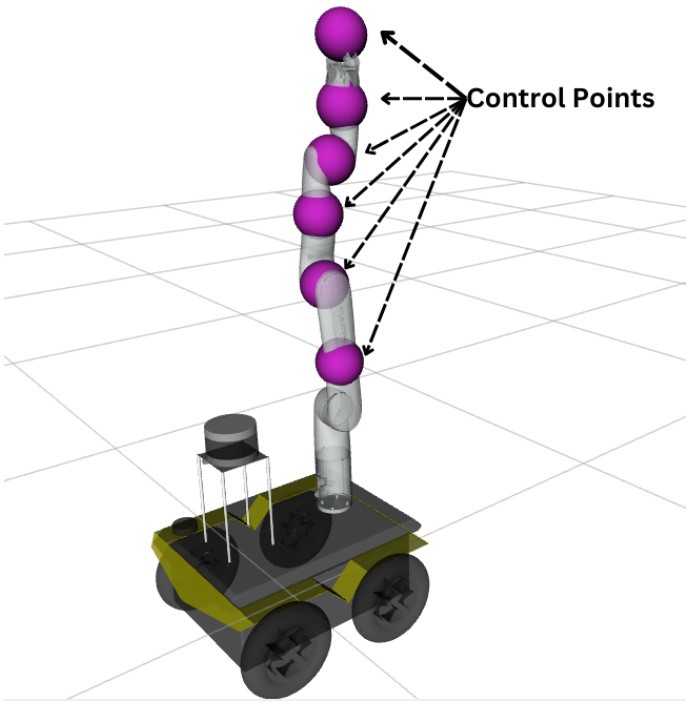

Figure 3.7: Visualization of the Control Points

Symbolic Name	Position	Frame
Control Point 0	Mid Arm	Mid of the link between Actuators 2-3
Control Point 1	Forearm	Actuator 3
Control Point 2	Lower Wrist	Actuator 4
Control Point 3	Upper Wrist	Actuator 5
Control Point 4	Gripper Base	Actuator 6
Control Point 5	End Effector	Tool

Table 3.1: Control Points Positions

This method allows the robot to follow the negative gradient of the potential function in real time, making it suitable for dynamic environments. We can say that we are using a virtual velocity field (VVF).

Repulsive virtual velocities are applied to all control points to ensure the arm avoids collisions with obstacles. However, for the attractive velocity guiding the robot toward the goal, only the control point located at the End Effector is influenced. This design creates a "follow-the-leader" motion: the End Effector, acting as the leader, is swiftly drawn to the target position, while the rest of the robot reorients itself to ensure all control points reach their intended final positions.

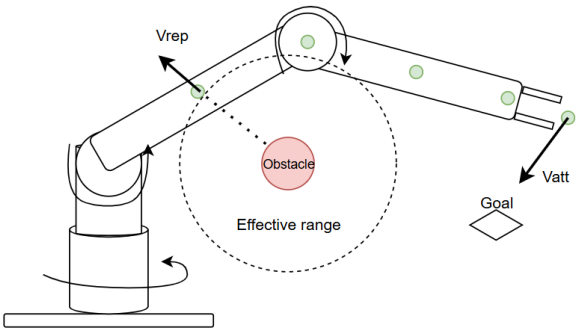

Figure 3.8: Virtual velocities

Attractive Velocity function

The attractive velocity function V_{att} generates a velocity vector pulling the manip-

ulator's End Effector toward the goal position p_{goal}.

$$V_{att} = \begin{cases} \zeta(p_{\text{goal}} - p_{end}), & d(p_{goal}, p_{end}) \leq d_0, \\ \zeta d_0 \frac{(p_{\text{goal}} - p_{end})}{d(p_{goal}, p_{end})}, & d(p_{goal}, p_{end}) > d_0. \end{cases} \tag{3.19}$$

where:

- p_{goal} is the goal position,
- p_{end} is the current End Effector position,
- ζ scales the magnitude of attraction,
- d_0 is the threshold distance for switching between the two potentials.

Smooth Speed Growth at the Beginning of Motion

A limitation of the standard attractive velocity function is that it immediately assigns a velocity vector, leading to an instantaneous jump in speed. This is unrealistic in real-world robotic systems.

To ensure a smooth increase in speed, we introduce an exponential scaling function that modulates the magnitude of the velocity over time:

$$V_{\text{att}} = \left(1 - e^{-kt}\right) \zeta d_0 \frac{(p_{\text{goal}} - p_{\text{end}})}{d(p_{\text{goal}}, p_{\text{end}})}. \tag{3.20}$$

where:

- $\left(1 - e^{-kt}\right)$ is the scaling function, which smoothly transitions from 0 to 1 as time progresses.
- k is a smoothing factor that determines how quickly the speed reaches its desired value.
- t is the elapsed time since the motion started.

Choosing the Smoothing Parameter k

The parameter k is selected based on the desired initial acceleration, following:

$$k = \frac{a_{\text{initial}}}{V_{\text{start}}}.$$

where:

- a_{initial} is the desired initial acceleration,
- V_{start} is the initial speed based in the attractive function (ζd_0).

To illustrate the effect of this smooth function, we present an example using specific parameter values: $\zeta = 0.35$, $d_0 = 0.2$, an initial acceleration of $a_{\text{initial}} = 0.05$ m/s^2, and an initial velocity given by $V_{\text{start}} = \zeta d_0 = 0.07$ m/s. The corresponding velocity and acceleration profiles are shown in Figure 3.9.

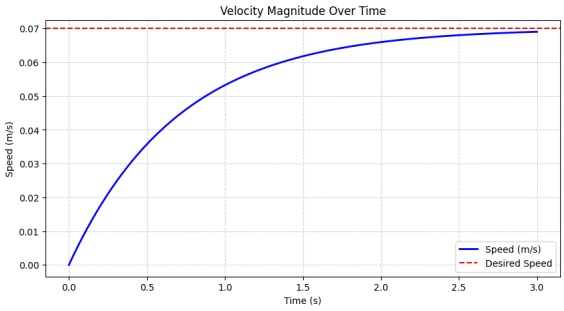

(a) Velocity Magnitude Over Time

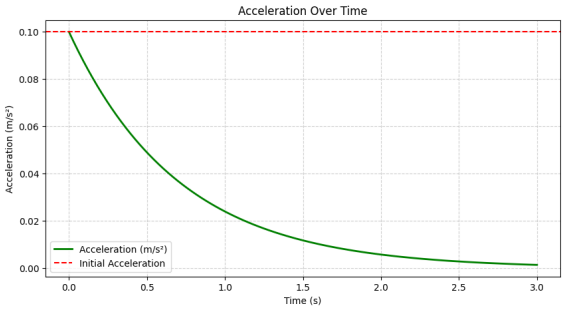

(b) Acceleration Over Time

Figure 3.9: Smooth Speed and Acceleration Profiles for Gradual Motion Initialization.

Repulsive Velocity function

The repulsive velocity function $V_{\text{rep},i}$ is defined for the closest control point p_j of the manipulator with respect to each obstacle O_i. It generates velocities to steer the robot away from obstacles, ensuring collision avoidance:

$$V_{\text{rep},i} = \begin{cases} -\eta \left(\frac{1}{Q_i^*} - \frac{1}{d_i(p_j)} \right) \frac{1}{d_i^2(p_j)} \nabla d_i(p_j), & d_i(p_j) \leq Q_i^*, \\ 0, & d_i(p_j) > Q_i^*, \end{cases} \tag{3.21}$$

where:

- $d_i(p_j)$ is the shortest distance between obstacle O_i and the closest control point p_j,
- Q_i^* is the influence threshold of the obstacle O_i,
- $\nabla d_i(p_j)$ is a unit vector pointing away from the obstacle,
- η scales the repulsive effect.

The repulsive velocity is generated only for the control point p_j that is closest to the obstacle O_i. Obstacles closer to the robot exert stronger influence, while those beyond Q_i^* have no effect.

Total Velocity Function

The total velocity is computed by combining the attractive and repulsive velocities and mapping them to the joint space using the Jacobian matrix. Each obstacle generates a repulsive velocity that influences only its closest control point. The combined velocities are then summed to compute the total repulsive effect. The process is described as follows:

Attractive Joint Velocity

The attractive velocity in joint space is calculated as:

$$\dot{q}_{\text{att}} = J_{\text{att}}^{-1}(q_{\text{end}}) V_{\text{att}}, \tag{3.22}$$

where J_{att} is the Jacobian matrix of the End Effector 2.4, q_{end} represents the joint configuration, and V_{att} is the attractive velocity in Cartesian space.

Repulsive Joint Velocity

The repulsive velocity in the joint space that an obstacle O_i generates at its closest control point p_j is given by:

$$\dot{q}_{\text{rep},i} = J_j^{-1}(q_m) V_{\text{rep},i}, \tag{3.23}$$

where J_j is the Jacobian matrix of the control point p_j, q_m represents the joint configuration of the manipulator (only the joints until the control point), and $V_{\text{rep},i}$ 3.21 is the repulsive velocity in Cartesian space generated by the obstacle O_i.

Aggregate Repulsive Velocity

The combined repulsive velocity in joint space is computed by summing the contributions from all obstacles:

$$\dot{q}_{\text{rep}} = \sum_{i=1}^{n} \dot{q}_{\text{rep},i}, \tag{3.24}$$

where n is the total number of obstacles.

Final Joint Velocity

The total velocity in joint space is the sum of the attractive and aggregate repulsive joint velocities:

$$\dot{q}_{\text{total}} = \dot{q}_{\text{att}} + \dot{q}_{\text{rep}}. \tag{3.25}$$

Execution Flow

The flow of the Traditional Artificial Potential Field (T-APF) method applied to the Manipulator is illustrated in Figure 3.10. The process follows a structured pipeline that allows the robot to compute its motion dynamically while considering attractive force toward the goal and repulsive forces from obstacles.

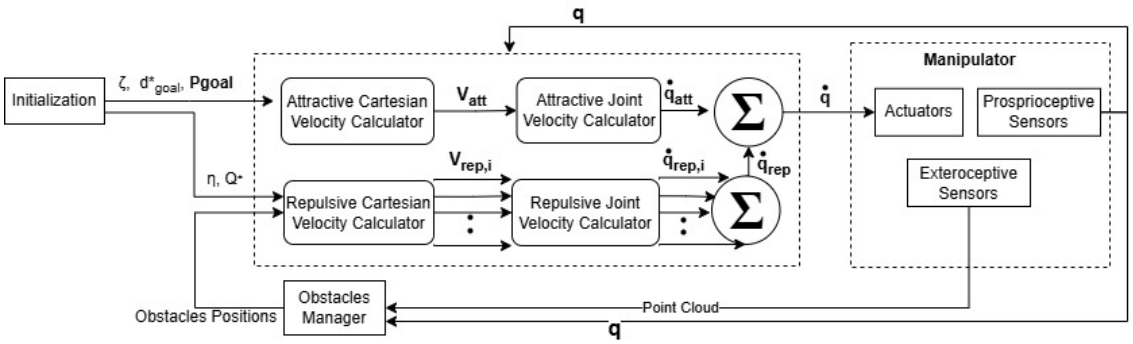

Figure 3.10: Execution flow of the Traditional APF Method

The implementation can be broken down into the following key stages:

- **Initialization:** The process begins with defining the goal position p_{goal} and the necessery parameters of the method such as the attractive strength ζ, the repulsive gain η, the d^*_{goal} and the obstacle influence threshold Q^*.

- **Obstacle Management:** The manipulator's environment is monitored using exteroceptive sensors, which detect obstacles and update their positions.

- **Attractive Velocity Computation:** The attractive Cartesian velocity V_{att} 3.19 is computed based on the current position of the End Effector relative to the goal. This velocity is then mapped to the joint space using the inverse Jacobian to obtain the joint velocities $\dot{q}_{\text{att}}$ 3.22.

- **Repulsive Velocity Computation:** The repulsive Cartesian velocities $V_{\text{rep},i}$ 3.21 are calculated for each control point affected by obstacles. These velocities are also mapped into the joint space using the inverse Jacobian of the control points to obtain the repulsive joint velocities $\dot{q}_{\text{rep}}$ (3.23 and 3.24).

- **Combining Velocities:** The attractive and repulsive joint velocities are summed to determine the total velocity $\dot{q}_{\text{total}}$ 3.25.

- **Manipulator Execution:** The computed joint velocities are sent to the actuators, which execute the movement. The proprioceptive sensors monitor joint configurations q, which are fed back into the method.

3.5 Simulation Analysis of T-APF

3.5.1 Obstacle-free environment

In this test case, we evaluate the implementation of the Traditional Artificial Potential Field (T-APF) method in an environment without obstacles. The robot's primary objective is to reach the goal position $p_{\text{goal}} = [0.6, 0.45, 0.4]$ (regardless the orientation) from its initial End Effector position $p_{\text{start}} = [0.5, -0.01, 0.77]$.

The parameters used in this test case are summarized in Table 3.2.

Parameter	**Symbol**	**Value**
Goal End Effector Position	p_{goal}	[0.6, 0.45, 0.4]
Start End Effector Position	p_{start}	[0.5, -0.01, 0.77]
Attractive Function Scaling	ζ	0.35
Attractive Threshold Distance	d^*_{goal}	0.2 m
Desired Initial Acceleration	a_{initial}	0.1 m/s^2

Table 3.2: Simulation parameters for the obstacle-free test case.

The motion is pictured into three stages in the figure below:

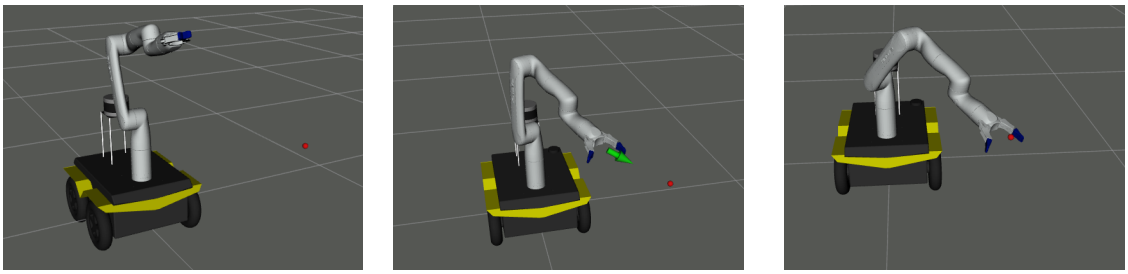

(a) Start position (b) Intermediate motion (c) Goal reached

Figure 3.11: Robot's movement towards the goal.
Live animation (GIF): github.com/GeorgiosSid/. . . /obstacle-free_environment.gif

Analysis of Test Case Data

The extracted data from the first test case provides key insights into how the arm moves towards its goal using the Traditional Artificial Potential Field (T-APF) method.

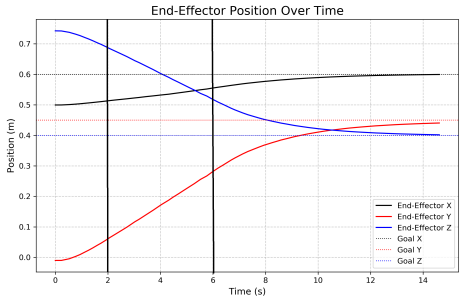

(a) End Effector position over time

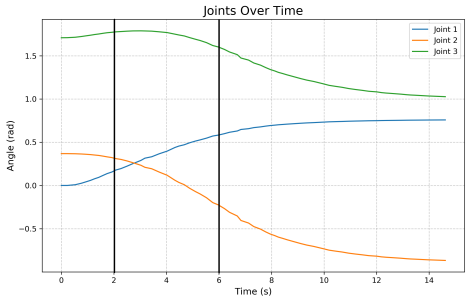

(b) Joint angles over time

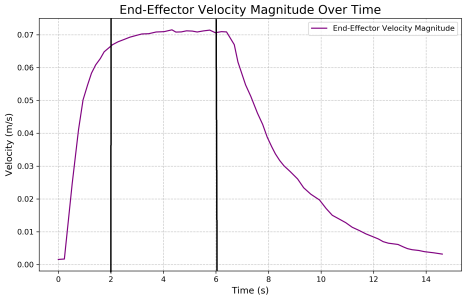

(c) End Effector velocity magnitude over time

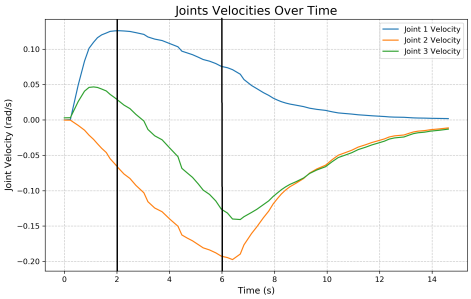

(d) Joint velocities over time

Figure 3.12: Analysis plots from the test case 1

Observations

- **End Effector Position Over Time:** The End Effector smoothly converges to the goal position. The final position for each axis is shown with dotted lines in the figure.
- **Joints Over Time:** A similar behavior is observed in the joint space, where the joint angles adjust smoothly to achieve the desired End Effector position.
- **End Effector Velocity Magnitude Over Time:** As seen in the figure, for the first 2 seconds, we observe the smooth start phase, where the velocity gradually increases until it reaches the desired constant speed of V_{start} =0.07 m/s (ζd^*_{goal}). From 2 to 6 seconds, the robot maintains this constant velocity, moving steadily toward the goal. Then, as the attractive function changes at

d^*_{goal}, the velocity gradually reduces to zero, ensuring a smooth stop near the goal.

- **Joint Velocities Over Time:** Similar velocity trends are observed in the joint space, where the velocity of each joint smoothly converges to zero near the goal.

This analysis confirms that the first test case was executed successfully, and the method is working correctly for simple goal-reaching tasks. Future test cases will introduce obstacles to further evaluate of the method.

3.5.2 Obstacle Influence on the End Effector

In this test case, we introduce an obstacle into the environment to analyze its influence on the robot's movement and evaluate the repulsive function of the Traditional Artificial Potential Field (T-APF) method. The repulsive function is applied only to the End Effector control point.

The parameters used in this test case are summarized in Table 3.3.

Parameter	**Symbol**	**Value**
Start End Effector Position	p_{start}	[0.62, 0.4, 0.4]
Goal End Effector Position	p_{goal}	[0.65, -0.4, 0.5]
Attractive Function Scaling	ζ	0.35
Threshold Distance for Attractive Function	d^*_{goal}	0.2 m
Repulsive Function Scaling	η	0.00023
Obstacle Influence Range	Q	0.15 m
Desired Initial Acceleration	a_{initial}	0.1 m/s^2

Table 3.3: Simulation parameters for the test case with an obstacle.

The obstacle is modeled as a cylinder with the following properties:

- **Center Position:** $[0.98, -0.04683, 0.46599]$
- **Radius:** 0.26583 m
- **Height:** 0.93198 m

The movement of the robot in this test case is illustrated in three key snapshots, as represented in Figure 3.13 below:

- **Initial Position:** The robot starts from its predefined position, with the obstacle clearly visible in the environment.
- **Intermediate Motion:** The robot moves towards the goal while avoiding the obstacle. The target position is shown as a red sphere, and three arrows illustrate the velocity components: the attractive velocity (green) directed towards the goal, the repulsive velocity (red) generated due to the obstacle, and the resultant velocity (blue), which dictates the final movement. The obstacle is visualized as a point cloud with red-colored points.
- **Final Position:** The robot reaches its goal after successfully navigating around the obstacle.

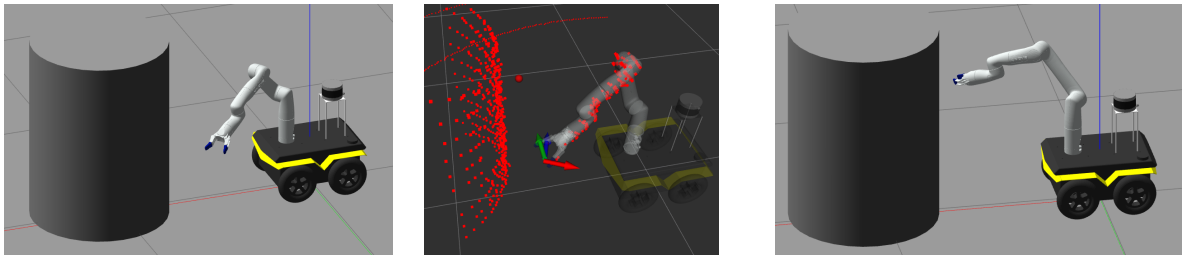

(a) Initial Position (b) Intermediate Motion (c) Final Position

Figure 3.13: Robot's movement towards the goal in the presence of an obstacle.
Live animation (GIF):
github.com/GeorgiosSid/. . . /Obstacle_Influence_on_End_Effector_gazebo.gif

Analysis of Test Case Data

We analyze the data from the second test case, where an obstacle influenced the End Effector's motion. Figure 3.14 shows key plots of the robot's trajectory,

velocity, and joint movements, highlighting the effect of the repulsive potential on its path.

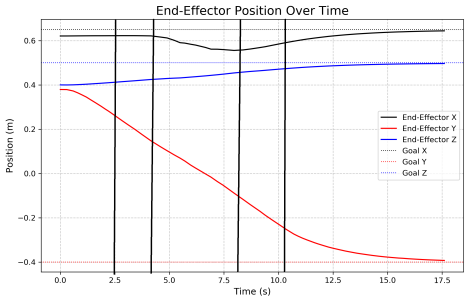

(a) End Effector position over time

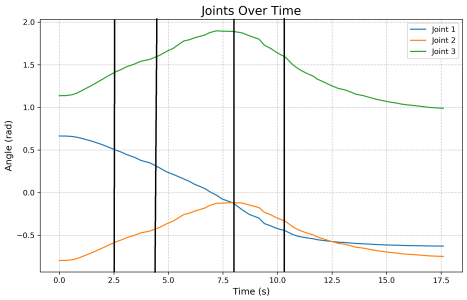

(b) Joint angles over time

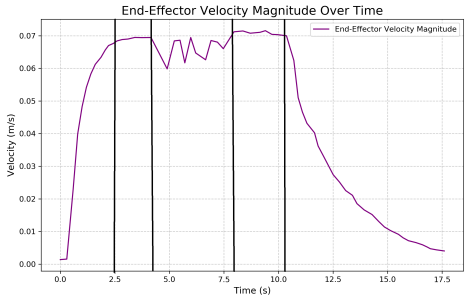

(c) End Effector velocity magnitude over time

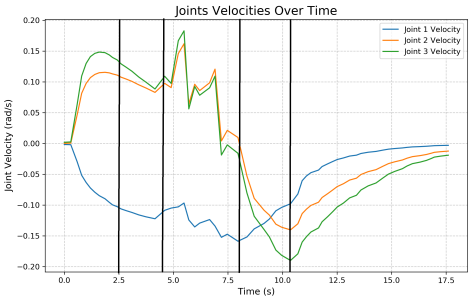

(d) Joint velocities over time

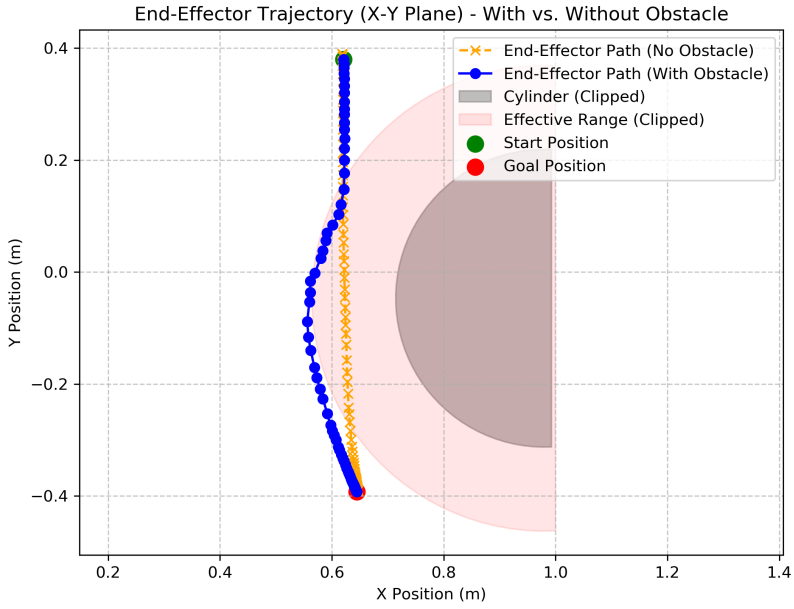

(e) End Effector Trajectory in X-Y Plane

Figure 3.14: Analysis plots from the test case 2

Observations

- **End Effector Position Over Time:** The End Effector smoothly converges to the goal position. The final position for each axis is indicated by dotted lines in the figure.

- **Joints Over Time:** A similar adaptation is observed in the joint space, where the joint angles adjust smoothly to achieve the desired End Effector position.

- **End Effector Velocity Magnitude Over Time:** The plot highlights three distinct phases. In the first 0 to 2.5 seconds the End Effector speed gradually increases until it reaches the desired constant speed of V_{start} =0.07 m/s (ζd^*_{goal}). The second phase (4 to 8 seconds) shows variations in velocity magnitude due to the obstacle's influence. After 10.5 seconds, the velocity gradually decreases to zero, ensuring a smooth stop at the goal position.

- **Joint Velocities Over Time:** A similar trend is observed in the joint velocity plot. During the obstacle influence period (4 to 8 seconds), the joint velocities adjust accordingly. As the End Effector nears the goal, joint velocities smoothly decrease to zero.

- **End Effector Trajectory in X-Y Plane:** The plot shows how the obstacle affects the End Effector's path. The change in the X-Y plane highlights the repulsive function's role in guiding the robot safely around the obstacle.

This analysis confirms that the T-APF's repulsive function, acting only on the End Effector, effectively ensures obstacle avoidance while reaching the goal. Future tests will explore its impact on other control points, ensuring safe navigation for the entire manipulator.

3.5.3 Multiple Obstacles Influence Different Control Points

In this test case, we introduce multiple obstacles in the environment, each affecting different control points of the manipulator. Unlike the previous case where only

the End Effector was influenced, here we analyze how the repulsive potential fields influence different parts of the robot.

The parameters used in this test case are summarized in Table 3.4.

Parameter	**Symbol**	**Value**
Start End Effector Position	p_{start}	[0.62, 0.4, 0.4]
Goal End Effector Position	p_{goal}	[0.65, -0.4, 0.5]
Attractive Function Scaling	ζ	0.35
Threshold Distance for Attractive Function	d^*_{goal}	0.2 m
Repulsive Function Scaling	η	0.00023
Obstacle Influence Range	Q	0.15 m
Initial Acceleration	a_{initial}	0.1 m/s^2

Table 3.4: Simulation parameters for the test case multiple obstacles.

The environment contains two obstacles, an cylinder and a sphere, each influencing different control points of the robot:

- **Obstacle 1 (Cylinder)**
  - **Center Position:** $[0.98, -0.04683, 0.46599]$
  - **Radius:** 0.26583 m
  - **Height:** 0.93198 m
  - **Influenced Control Point:** End Effector
- **Obstacle 2 (Sphere)**
  - **Center Position:** $[0.531653, -0.038728, 0.9]$
  - **Radius:** 0.1703 m
  - **Influenced Control Point:** Lower Wrist

The robot's motion through the environment is depicted in Figure 3.15, showing three distinct stages:

- **Initial Position:** The robot starts from its predefined position, with the obstacles clearly visible in the environment.
- **Intermediate Motion:** In this figure, the robot is in an intermediate state where the End Effector is influenced by the cylindrical obstacle, while at the same time, the lower wrist is affected by the spherical obstacle. The repulsive (virtual velocity) forces generated by the obstacles at each control point are visualized as red arrows. Additionally, the obstacles are represented as a point cloud of white points.The green arrow represents the attractive velocity that is directing the End Effector towards the goal position.
- **Final Position:** In the final figure, we can see that the manipulator has successfully reached its goal position, navigating around the cylindrical obstacle and passing underneath the spherical obstacle.

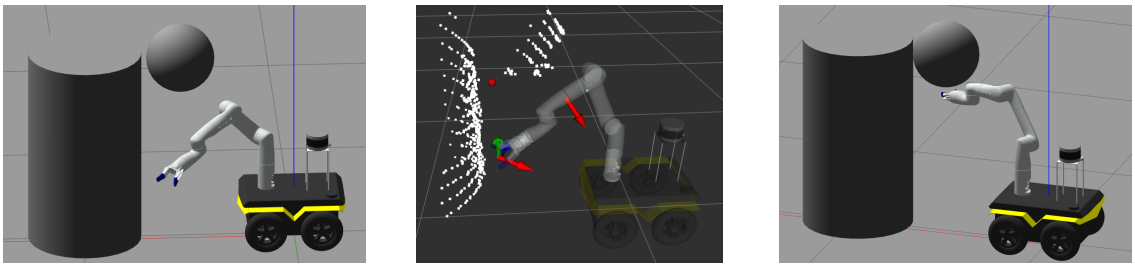

(a) Initial Position (b) Intermediate Motion (c) Goal Reached

Figure 3.15: Robot's movement towards the goal while avoiding multiple obstacles.

Live animation (GIF):
github.com/GeorgiosSid/.../Multiple_Obstacles_Influence_Different_Control_Points_gazebo.gif
Live animation (GIF):
github.com/GeorgiosSid/.../Multiple_Obstacles_Influence_Different_Control_Points_rviz.gif

Analysis of Test Case Data

The following plots provide a deeper understanding of how the robot reacted to multiple obstacles and adjusted its path:

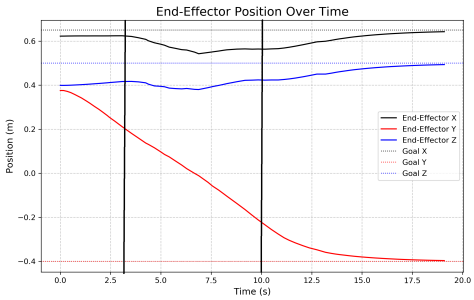

(a) End Effector position over time

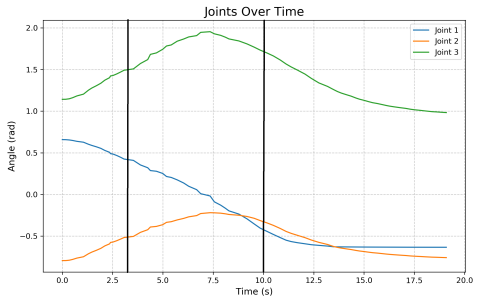

(b) Joint angles over time

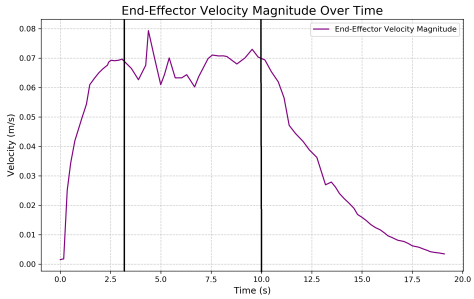

(c) End Effector velocity magnitude over time

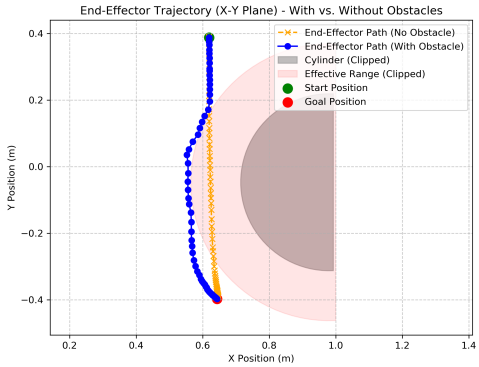

(d) End Effector Trajectory in X-Y Plane

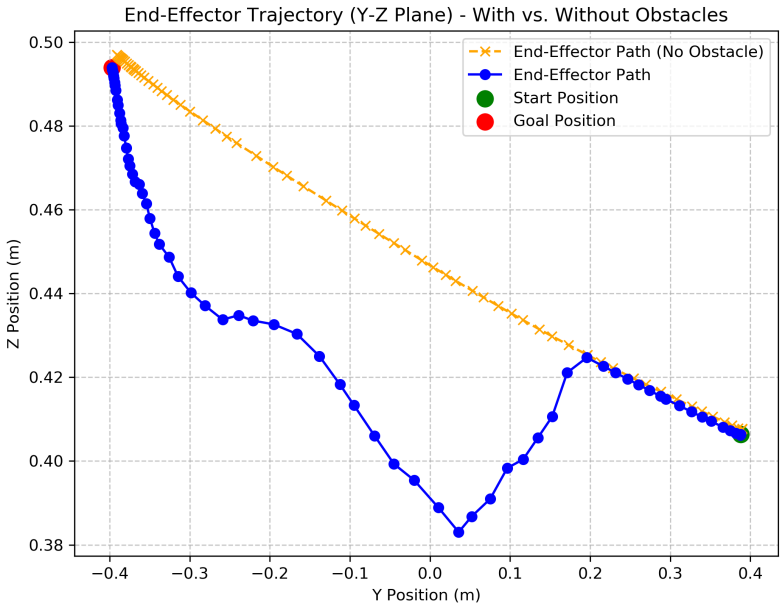

(e) End Effector Trajectory in Y-Z Plane

Figure 3.16: Analysis plots from the test case 3

Observations

- **End Effector and Joints Position Over Time:** The End Effector and in

the same time the joins smoothly converges to the goal position.

- **End Effector Velocity Magnitude Over Time:** Similar to the second test case, the velocity profile highlights three distinct phases. Initially, the End Effector smoothly accelerates to 0.07 m/s (ζd^*_{goal}). During the obstacle avoidance phase (between 3 to 10 seconds), speed variations occur as the repulsive field influences the movement. Finally, as the robot nears the goal, velocity smoothly decreases to zero.

- **End Effector Trajectory in X-Y Plane:** The influence of the cylindrical obstacle on the trajectory of the End Effector in the X-Y plane can be observed, as it alters its path to avoid the obstacle.

- **End Effector Trajectory in Y-Z Plane:** The spherical obstacle affects the End Effector's path in the Y-Z plane by influencing the lower wrist control point, causing the manipulator to adjust its movement.

This analysis demonstrates that when multiple obstacles influence different control points, the Traditional Artificial Potential Field (T-APF) method enables safe navigation while still reaching the goal.

3.6 Real-World Experimentation